Using Cation Exchanged Nanorod Templates to Direct the Regioselective Growth and Plasmonic Coupling of Gold Nanoparticles

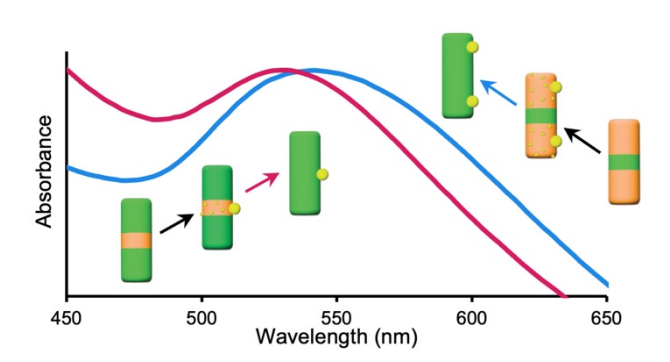
Joseph M. Veglak,¹ Chul-Hyun Jeong,¹ Haley L. Young,¹ Sarah K. O'Boyle,¹ and Raymond E. Schaak^{1,2,3,*}

E-mail: res20@psu.edu

ABSTRACT

Plasmonic coupling of gold nanoparticles results in a red shift of the plasmon peak in the visible absorption spectrum, resulting in a color change that is sensitive to the interparticle spacing. Here, we used multiple sequential partial cation exchange reactions to design heterostructured nanorod templates that define the regions onto which gold nanoparticles photodeposit. Starting with nanorods of copper sulfide (Cu_{1.8}S), we synthesized ZnS–CdS, CdS–ZnS–CdS, and ZnS–CdS–ZnS nanorods. Illumination with a blue LED light initiated photodeposition of Au nanoparticles selectively onto the CdS regions. Subsequent cation exchange reactions transformed the CdS regions to Cu_{1.8}S and then to ZnS while also facilitating surface diffusion and migration of the photodeposited Au, which coalesced into single particles through a surface ripening process. This process produced nanorods that were fully ZnS but with Au nanoparticles anchored in distinct regions. The Au–ZnS–Au sample exhibited a red shift of the plasmon peak relative to Au–ZnS due to plasmonic coupling of the Au particles on the ZnS nanorod support.

Table of Contents Graphic



¹ Department of Chemistry, ² Department of Chemical Engineering, and ³ Materials Research Institute, The Pennsylvania State University, University Park, PA 16802.

The ability to precisely place one type of nanoparticle on the surface of another is a prerequisite for engineering photonic nanostructures that couple together multiple optically active components, such as multi-component chiral,¹ nonlinear optical,²-5 and photocatalytic architectures.⁶⁻⁹ The controlled coupling of nanoparticles is commonly achieved using several strategies. Individual colloidal nanoparticles can be connected to one another through surface molecule interactions, including chemically selective linkers such as DNA.¹0-12 One type of nanoparticle can seed the growth of another, producing hybrid nanoparticles having directly coupled solid-state interfaces.¹3-17 Other colloidal methods can modify nanoparticle composition in certain regions, producing interfaced materials and heterostructures.¹6,18-21 Nanoparticles can also be deposited on planar surfaces using nanolithography and electron beam lithography to generate periodic arrays with controlled spacings and arrangements.⁴,22-24 Additionally, AFM tips can physically move Au nanoparticles closer together on a surface to control their relative spacings.⁵

These and other approaches provide pathways for generating optically coupled nanoparticle constructs. In some cases, regioselective placement is possible, whereby the relative locations of two or more coupled nanoparticles can be controlled. For example, different regions of a nanocrystal surface having different energies can have different reactivities that influence where the seeded growth of a new nanoparticle will preferentially occur. The placement of metal nanoparticles selectively at the tips of CdS nanorods and the growth of hierarchical nanostructures through facet-selective deposition demonstrate this approach.²⁵ Photodeposition of metals onto nanoparticles that incorporate multiple semiconductors, such as CdSe–CdS, can occur on one material versus the other due to differences in band gap energy.²⁶ Despite these capabilities, regioselective growth of one type of nanoparticle on the surface of another remains challenging.

Here, we introduce a strategy for designing heterostructured nanoparticles that facilitates the regioselective placement of Au nanoparticles at desired locations on the surface of ZnS nanorods. This method, shown schematically in Figure 1, begins with using well-established cation exchange chemistry to introduce intraparticle frameworks of different semiconductors (ZnS, CdS) into colloidal nanorods at predetermined locations, which subdivides them into chemically, optically, and electronically distinct regions. 19,20,27,28 We begin with nanorods of roxbyite copper sulfide, Cu_{1.8}S, and then exchange a fraction of the Cu⁺ cations with Zn²⁺, which results in regions of ZnS segregated within the Cu_{1.8}S nanorods. Next, we exchange the remaining Cu⁺ cations with Cd²⁺, which retains the interfaces, replaces the remaining Cu_{1.8}S with CdS, and forms heterostructured ZnS-CdS nanorods. The arrangements of the ZnS and CdS regions - ZnS nanorods with a single CdS tip, double CdS tips, and a CdS central band – are defined during the first partial cation exchange step and are tunable and predictable based on established design rules, described below. We then photodeposit Au nanoparticles selectively on the CdS regions by leveraging the differences in their band gap energies. When the material having the smaller band gap, CdS, is illuminated with light having a wavelength greater in energy than its band gap but lower in energy than the band gap of ZnS, the CdS will selectively absorb photons to excite and confine electrons to the conduction band. These excited electrons can then be used to reduce the Au at the surface, keeping it localized to the CdS region. Through a series of additional cation exchange reactions, we then remove the intraparticle frameworks and convert the entire rod to ZnS, while the Au remains anchored in the region where it was initially deposited. This multi-step process results in ZnS nanorods that have Au nanoparticles selectively deposited near the tips. near the middle, or near both tips; the latter exhibit coupled plasmonic properties that mimic those

produced by other methods, such as DNA linking, but in a discrete colloidal nanoparticle construct that was engineered without organic or biomolecular linkers.

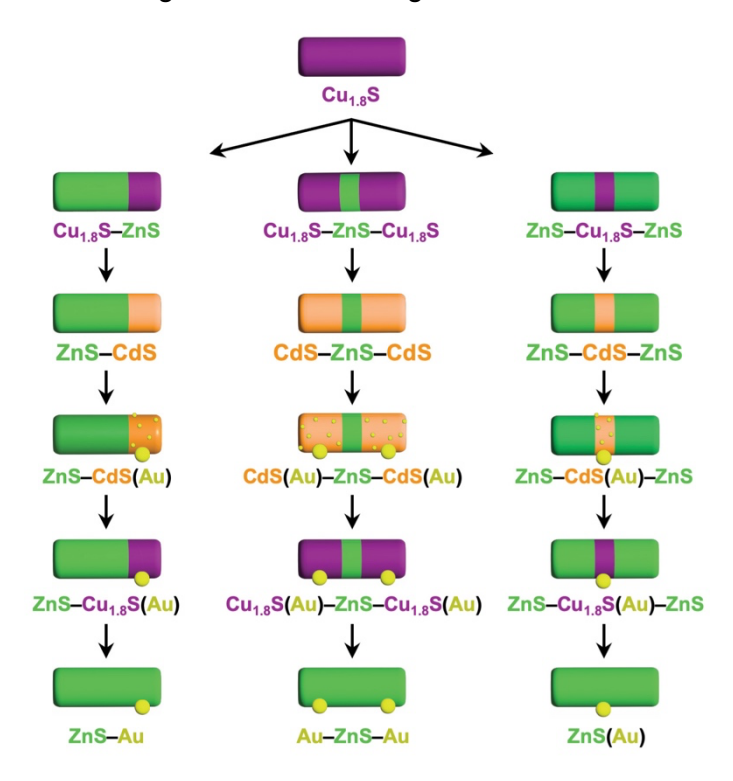


Figure 1. Schematic depicting the multi-step sequence of partial cation exchange reactions and photodeposition steps that lead to the rational synthesis of ZnS nanorods with regioselective placement of one or two Au nanoparticles.

Starting with roxbyite Cu_{1.8}S nanorods (Figure S1),¹⁹ three different ZnS–CdS heterostructured nanorod derivatives were synthesized using various sequences of partial cation exchange reactions, as detailed in the Supporting Information. Figure 2 includes HAADF-STEM images and corresponding STEM-EDS element maps of Cd and Zn for all three types of nanorods, confirming the intended spatial distributions of CdS and ZnS; additional STEM-EDS element maps are shown in Figures S2-S4. X-ray diffraction (XRD) analysis, including peak positions, peak widths, and relative intensities, also confirmed the presence of wurtzite ZnS and CdS in the nanorods (Figure S5).

For the ZnS nanorods having a single tip of CdS, analysis of 144 particles revealed that 85% were ZnS–CdS single-tipped rods, with the remainder consisting primarily of CdS–ZnS–CdS double-tipped nanorods. For the double-tipped CdS–ZnS–CdS nanorods, 62% of 476 nanorods observed consisted of the targeted CdS–ZnS–CdS heterostructure, with the remainder being composed of single-tipped ZnS–CdS nanorods. For the ZnS–CdS–ZnS nanorods, which have a central band of CdS, analysis of 187 particles indicated that 92% were the targeted ZnS–CdS–ZnS nanorods, with the remainder containing multiple stripes of CdS, *i.e.*, ZnS–CdS–ZnS–CdS–ZnS (Figures 2 and S6-S8 show STEM-EDS elemental maps containing all counted particles.). The synthetic protocols used to generate these three distinct classes of ZnS–CdS nanorods leverage both

existing knowledge and new modifications, both discussed in the Supporting Information, that help to direct exchange to precise locations.

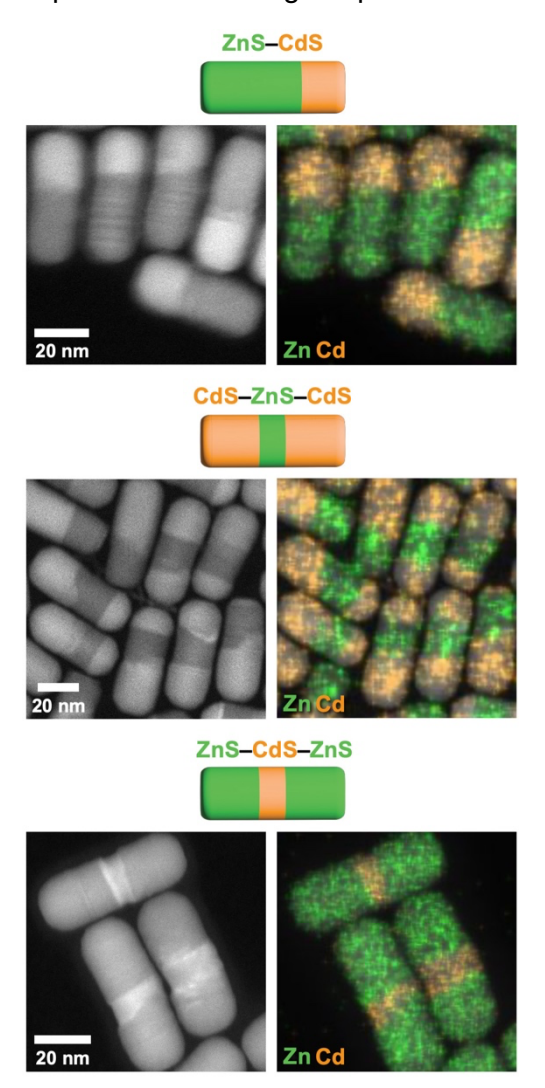


Figure 2. For each of the three ZnS/CdS heterostructured nanorod templates (single tip ZnS–CdS, double tip CdS–ZnS–CdS, and central band ZnS–CdS–ZnS), HAADF-STEM images are shown in the left and overlayed STEM-EDS element maps are shown on the right. (Green = Zn $K\alpha$, orange = Cd $L\alpha$)

With these three distinct samples of ZnS–CdS nanorods in hand, we next sought to grow Au selectively on the CdS regions. We first evaluated the growth of Au on ZnS and CdS nanorods separately to identify appropriate reaction conditions and to serve as a series of control experiments, as shown by the XRD and TEM images in Figure 3. Nanorods of CdS, which as a bulk material has a band gap of 2.4 eV that is slightly lower in energy than the 2.6 eV of the 470-nm LED lights used for irradiation, were able to photoreduce Au when irradiated for 8 minutes. The TEM image in Figure 3b confirms that particles deposited on the CdS nanorods and the XRD data in Figure 3a indicates that Au is present. As expected for ZnS, where the incoming light had an energy smaller than the band gap, Au would not grow. Nanorods of ZnS, which as a bulk

material has a band gap of 3.6 eV that lies in the ultraviolet region, did not grow Au, based on the lack of Au by XRD and the lack of deposited particles by TEM (Figures 3a and 3c). Even when using a UV-emitting lamp as a light source, the ZnS nanorods did not grow Au after 8 minutes, as indicated by the lack Au by both XRD (Figure 3a) and TEM (Figure 3d). Increasing the irradiation time with the UV-emitting lamp to 1 hour resulted in photoreduction of Au on the ZnS nanorods (Figures 3a and 3e). It is worth noting in these control experiments that for the rods that were able to grow Au, the placement of the Au appeared random (Figure 3b and 3e). There was some preference toward Au nanoparticle growth on or near the nanorod tips, as is well known to occur in such systems, ^{29–32} but Au was also frequently present at other locations around the nanorods. Additionally, on initial inspection, many CdS nanorods did not appear to have any Au present. However, at higher magnifications, these nanorods were found to contain many small Au particles all over the surface (Figure 3b, inset). This behavior is also commonly observed during photoinduced Au growth. ^{29,32,33}

These control experiments established that nanorods of CdS would seed the growth of Au when illuminated with 470-nm blue LED light for 8 minutes while under identical conditions, ZnS nanorods would not. We then applied these growth conditions to the three types of heterostructured nanorods shown in Figure 2 to selectively grow Au on the CdS regions. Figure 4a shows STEM-EDS element maps for Cd, Zn, and Au, which confirm that Au nanoparticles photodeposited onto the nanorods and that they sit adjacent to the CdS regions and not the ZnS regions. (Some Au nanoparticles appear near the CdS–ZnS interface but are connected to the CdS region. Others that appear to be adjacent to ZnS are actually connected to CdS regions on neighboring nanorods, *i.e.*, their apparent location next to ZnS is an artifact of how the nanorods sit next to each other.) Individual STEM-EDS element maps are included in Figures S9-S12. These results provide strong evidence that the photodeposited Au is localized to the CdS regions and excluded from the ZnS regions. Additionally, the XRD data in Figure S13 helps to validate key materials characteristics of the Au/CdS/ZnS nanorods in the bulk sample; a detailed discussion is provided in the Supporting Information.

At this point, we have three distinct samples of heterostructured nanorods containing ZnS and CdS with Au deposited selectively on the CdS regions. However, our goal is to use the ZnS/CdS nanorods as templates to control where the Au photodeposits, but ultimately have the nanorods consist of only ZnS, so that the final system has only one type of nanoparticle (Au) that absorbs at visible wavelengths. To achieve this goal, we sought to replace the Cd2+ with Zn2+ to transform the CdS to ZnS, making the entire rod consist of ZnS. However, the chemical driving force for cation exchange, which includes hard-soft acid-base interactions, does not allow this exchange to proceed directly, since Cd2+ and Zn2+ do not differ substantially in their hardness values. Instead, we carried out an intermediate exchange of Cd²⁺ with Cu⁺ to replace the CdS with Cu_{1.8}S, followed by exchange of the Cu⁺ in Cu_{1.8}S with Zn²⁺ to transform the Cu_{1.8}S (that used to be CdS) to ZnS. This sequence, which transforms (as one example) CdS–ZnS to Cu_{1.8}S–ZnS and then to ZnS-ZnS, is possible based on the existing knowledge that Cd2+ in CdS will exchange with Cu+ but Zn²⁺ in ZnS will not.³⁷ Figure 4a shows STEM-EDS element maps that confirm the replacement of Cd2+ with Cu+ to form Cu1.8S without disrupting the spatial localization of the photodeposited Au nanoparticles; individual STEM-EDS element maps are provided in Figures S14-S16. The Au particles were previously on the CdS regions, and after Cu⁺ exchange, they remain in the same regions, which now consist of Cu_{1.8}S. Finally, the Cu⁺ cations in the Cu_{1.8}S regions were fully replaced with Zn²⁺ to transform them to ZnS, as confirmed by STEM-EDS data in Figure 4a, resulting in nanorods that are fully ZnS; individual STEM-EDS element maps are

provided in Figures S17-S19. The XRD data in Figure S13 further validate the success of these cation exchange reactions throughout the bulk sample.

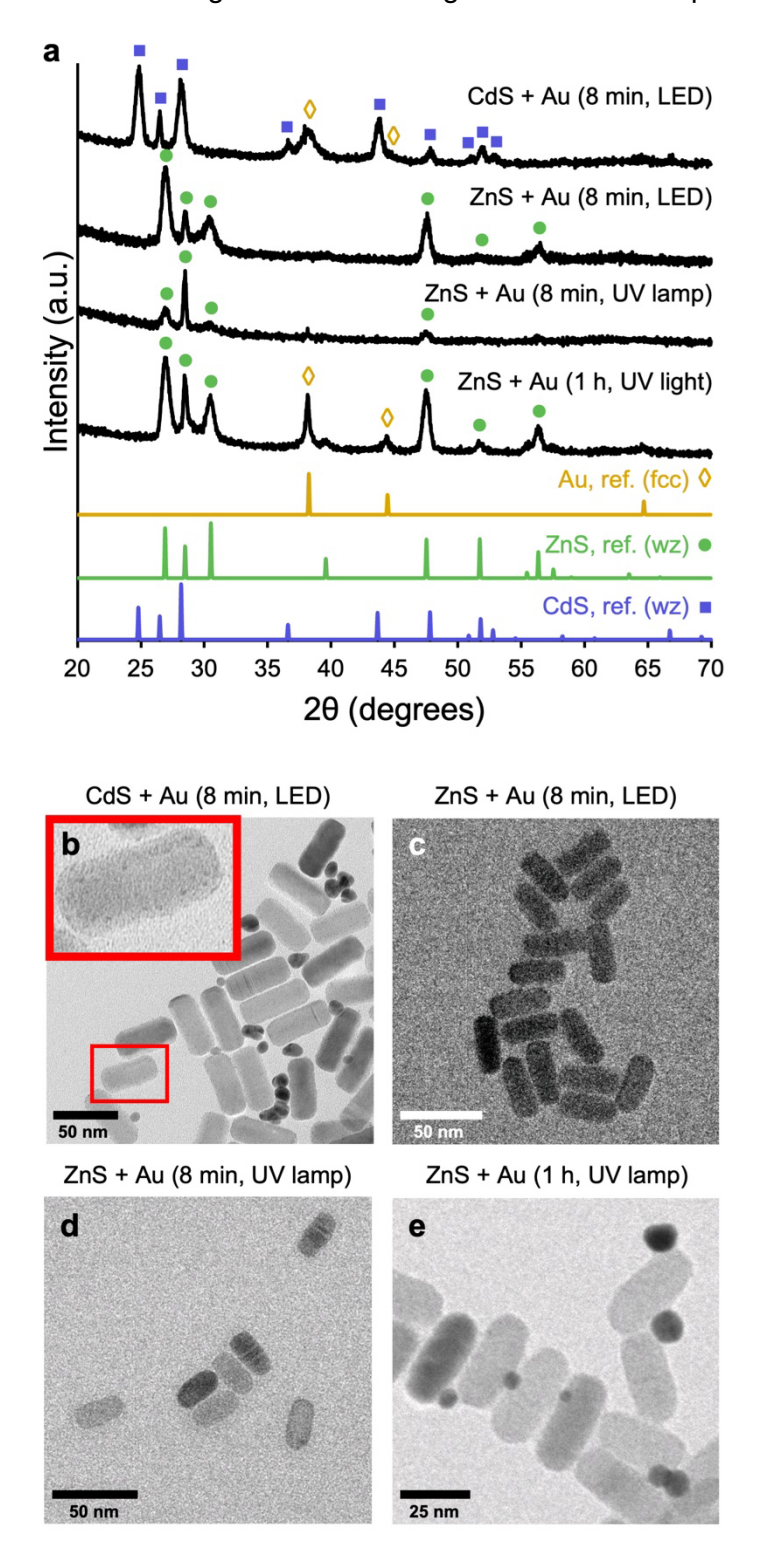


Figure 3. (a) XRD and (b-e) TEM data that confirms the presence or absence of Au photodeposition in control samples. The four control samples are nanorods of (b) CdS that have

been irradiated with blue LED light for 8 minutes, (c) ZnS that have been irradiated with blue LED light for 8 minutes, (d) ZnS irradiated with a UV-emitting lamp for 8 minutes, and (e) ZnS irradiated with a UV-emitting lamp for 1 hour. In (a), simulated reference patterns of fcc-Au,³⁴ wurtzite ZnS,³⁵ and wurtzite CdS³⁶ are shown for comparison. The inset in (b) highlights the smaller dark spots ("speckling") on the CdS nanorods, which are from the photodeposition of small Au particles across the surface of the nanorods.

The data in Figure 4b provide additional insights into how the photodeposition of Au occurs selectively on the CdS regions and how the subsequent exchanges with Cu⁺ and Zn²⁺ impact it. As discussed earlier, control experiments showed that Au photodeposition on CdS produced large amounts of small Au nanoparticles speckled across the entire CdS surface (Figure 3b). Similar behavior is observed during Au photodeposition on ZnS–CdS, as brighter spots corresponding to smaller Au particles can be seen speckled all over the CdS regions in the HAADF-STEM images in Figure 4b (top). However, after the Cu⁺ exchange that transforms the CdS–ZnS nanorods to Cu_{1.8}S–ZnS, the Au appears to have coalesced into a single domain on each nanorod, as noted by the lack of brighter contrast regions in the corresponding HAADF STEM images (Figure 4b (bottom). The single Au domain remains after Zn²⁺ exchange. This behavior is consistent with an Ostwald ripening process, whereby the larger Au particle grows at the expense of the smaller ones, which coalesce through diffusion across the surface.³⁰

As mentioned previously, this speckling of Au on CdS is not uncommon for nanoparticle systems where Au is grown on CdS. ^{29,32} Truly single tipped Au–CdS nanorods, having a minimal number of speckled Au-CdS particles as a side product, have been previously synthesized. In one example, two experimental strategies were critical to achieving single tipped Au-CdS.³³ First, methanol was used as a hole scavenger to reduce the likelihood of electrons becoming trapped at surface defects, which would increase the probability of nucleating multiple Au nanoparticles. Second, a high power (>100 mW/cm²) laser was used as the light source, and this was likely to increase the total number of excited electrons so that the Au can be more readily reduced onto the surface of the larger and growing Au nanoparticle. As an alternative, we additionally considered the possibility that higher laser powers could also heat the nanorods, which would enhance the diffusion of Au along the surface of the nanorod and help to facilitate Ostwald ripening. However, in previous studies of Au growth on CdS nanorods through both thermally and light driven processes, the thermally driven processes generally favor speckling of small Au particles on the CdS nanorod surface, even when combined with illumination of the particles using blue light. Regardless, it is not unreasonable to expect large amounts of small Au particles speckling the surface of our nanorods during photodeposition using low-power LED illumination.

Rather than requiring a high-power laser to grow single domains of Au onto a nanorod, the data in Figure 4b suggest that the Cu⁺ back exchange reaction enables migration of the Au. We speculate that during the exchange step involving the replacement of Cd²⁺ with Cu⁺, the rapid movement associated with the cations diffusing in and out of the nanorod allows for easy migration of the Au across the surface. The result of this process is to form a single larger particle that would be energetically more stable than many smaller domains. Cation exchange necessarily requires the surface to be dynamic, given that it is the entry and exit point for incoming and outgoing cations, respectively, and the ligands are concomitantly dynamic. Further support for this process comes from analysis of the CdS–ZnS–CdS heterostructured nanorod onto which Au was photodeposited. Immediately following Au photodeposition, only a few of the CdS–ZnS–CdS

nanorods appeared to have two distinct Au domains. However, in the final product, which consisted of Au on only ZnS, a majority of the nanorods have two Au particles on them. Additionally, for nanorods having larger CdS regions onto which Au is photodeposited as speckled particles, the average size of the coalesced Au after replacing the Cd²⁺ with Cu⁺ is larger (Figure S20). This observation indicates that more Au photodeposits when the CdS surface area is higher, which leads to larger Au particles after surface migration and coalescence.

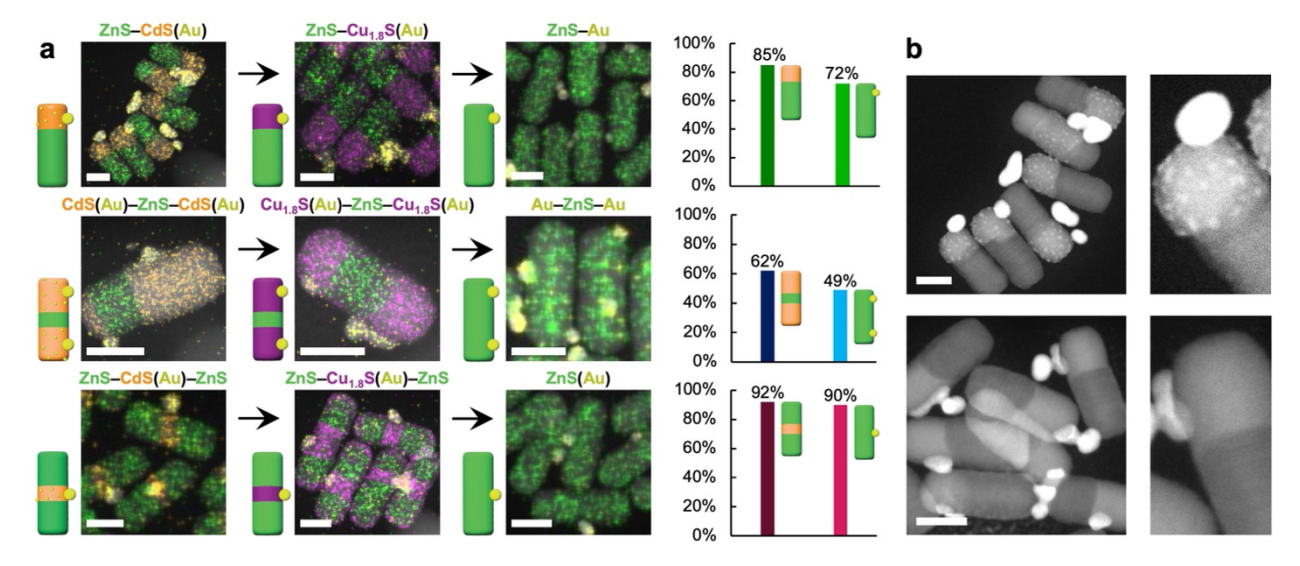


Figure 4. (a) STEM-EDS element maps characterizing each cation exchange step for each of the three types of ZnS/CdS heterostructured nanorod templates after Au photodeposition. These steps include (from left to right) the exchange of Cd^{2+} with Cu^{+} to transform the CdS regions to $Cu_{1.8}S$ and the exchange of Cu^{+} with Zn^{2+} to exchange the $Cu_{1.8}S$ regions to ZnS, ultimately forming nanorods that only contain ZnS and Au. (Green = Zn Kα, orange = Cd Lα, yellow = Au Lα, purple = Cu Kα.) The corresponding bar charts on the right track the percentage yields (based on counting statistics, as described in the text) of the starting heterostructured nanorod templates to the final Au/ZnS products. (b) HAADF-STEM images (two magnifications) showcasing the initial Au growth step on the single tipped CdS–ZnS nanorod (top), which corresponds to small Au nanoparticles speckled across the CdS surface of the CdS–ZnS nanorods, along with the same system after Cu^{+} exchange to form Au– $Cu_{1.8}S$ –ZnS, where the speckled Au has coalesced with the larger particles. All scale bars shown are 20 nm.

Categorizing and counting particles allowed us to correlate the location of the Au domains to the location of the CdS in the initial CdS/ZnS heterostructures, helping to validate retention of regioselectivity defined during photodeposition. For the single-tipped CdS–ZnS rods where 85% of the CdS was localized to the end of the rod, 72% (n=235) of the final ZnS/Au rods had the Au located within the top third of the nanorod (Figure 4a). The double-tipped sample, for which 62% of the nanorods were the targeted CdS–ZnS–CdS heterostructure, had 49% (n=176) of the product ZnS/Au nanoparticles containing two Au domains. Finally, in the nanorod sample for which 92% had a central band of CdS (ZnS–CdS–ZnS), 90% (n=187) of the product ZnS/Au rods had Au localized to the central third of the nanorod. Additional discussion of the product yields is provided in the Supporting Information, along with images of all of the particles counted in determining the Au domain placement (Figures S21-S23).

The ability to direct both the number and location of photodeposited Au nanoparticles, which have a visible-wavelength surface plasmon resonance, on ZnS nanorods, which are optically transparent at visible wavelengths, allows us to interrogate controlled plasmonic Au nanoparticle coupling on a solid-state support. It is known that the localized surface plasmon resonance (LSPR) in Au nanoparticles shifts to different wavelengths depending on the spacing between them. For Au particle spacings greater than 200 nm, the LSPR exhibits a blue shift that increases as particle spacing decreases. At much shorter Au particle spacings of 8-24 nm, which are generated by linking together Au nanoparticles with DNA strands, there is a red shift in the Au LSPR that increases with decreasing Au interparticle distance. 10-12

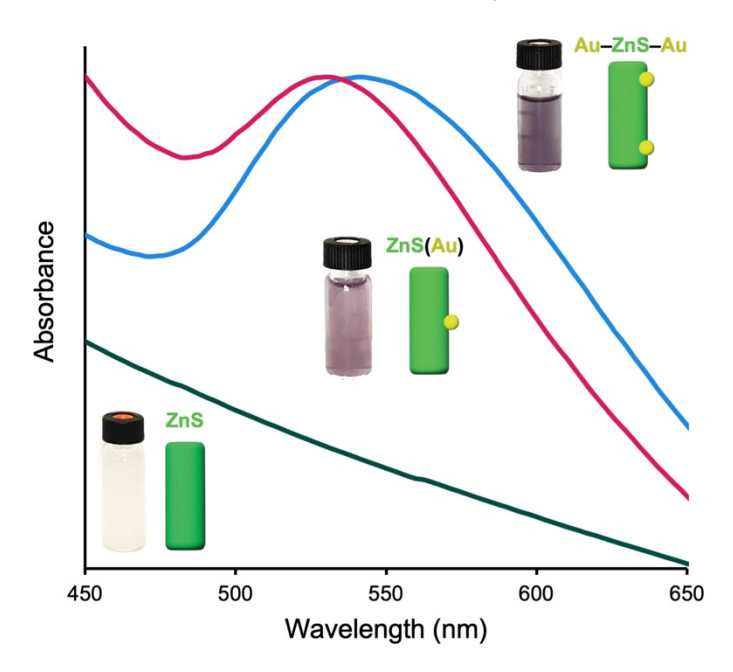


Figure 5. Visible absorption spectra showing the plasmon peak for the ZnS(Au) nanorods (red) and the Au–ZnS–Au nanorods (blue), which exhibit a red shift due to coupling of the two Au particles anchored to the ZnS nanorods. The corresponding visible absorption spectrum for ZnS nanorods without Au (green) are shown for comparison. The overlaid photographs show vials of colloidal suspensions of each sample, along with corresponding illustrations of the majority product in each vial.

All the methods referenced above for coupling together plasmonic Au nanoparticles require depositing particles at controlled spacings on surfaces or post-synthetically connecting them in ways that control their spacings. A drawback of these methods is their inability to control precisely how many particles are linked or whether they are also linked to another particle. Here, we anchor plasmonic Au particles regioselectively on colloidal ZnS nanorod supports to address these challenges. Two of the heterostructured nanorod precursors, CdS–ZnS and ZnS–CdS–ZnS, produce one Au particle per ZnS rod, *i.e.*, Au–ZnS, after back-exchange of Cd²⁺ with Cu⁺ and then Zn²⁺, while CdS–ZnS–CdS produces two Au particles per ZnS rod, which can be depicted (after full conversion to ZnS) as Au–ZnS–Au. Given consideration of the locations of the Au particles relative to each other on the two-particle ZnS rods, as well as their range of locations, the average spacings between the ZnS-anchored Au nanoparticles are 22 ± 9 nm, which fall within

the range of coupled nanoparticles that should exhibit a red shift relative to ZnS nanorods containing only one Au nanoparticle.

Experimental UV-visible absorption spectra, shown in Figure 5, validate these predictions about the LSPR based on the relative positions of the Au nanoparticles and also confirm that the particles are coupled throughout the bulk of the sample and therefore represent the majority product of the multi-step synthesis. For the measurements involving ZnS nanorods that contain a single Au particle, we chose to use the ZnS-Au nanorods with the Au located on the central third of the ZnS rod due to their higher yield. For these Au-ZnS nanorods, the maximum absorbance for the LSPR is around 530 nm. This value for the maximum absorbance is consistent with what we would expect to observe, as the ~12 nm Au particles alone would exhibit a maximum absorbance near 520 nm that would red shift by ~10 nm, to approximately 530 nm, when coupled with ZnS.³⁸ For the ZnS nanorods that contain two Au particles separated by an average distance of 22 ± 9 nm, the maximum absorbance exhibited a further red shift to 542 nm, which is consistent with the red shift observed for DNA-linked Au nanoparticles having a comparable interparticle distance of 24 nm and a red shift of 15 nm. 10 We further validated that the observed red shift arises from the proximity of Au nanoparticles and not from other factors that influence LSPR peak positions. First, we determined that the average Au particle diameters and standard deviations in both samples were identical at 10 ± 5 nm (n = 135 for Au–ZnS and n = 87 for Au–ZnS–Au). Second, Scherrer analysis of the XRD data for the Au-ZnS and Au-ZnS-Au samples indicated Au grain sizes of 12.5 nm and 12.7 nm, respectively, which are comparable to the particle sizes observed by TEM. It is worth noting that the UV-vis spectrum for the Au-ZnS-Au sample exhibits a slight shoulder around 530 nm, which is consistent with the particle counting data for this sample indicating that approximately half of the particles had two Au domains while the other half had only one; contributions from both subpopulations are therefore expected and observed.

In conclusion, we demonstrated the retrosynthetic design and regioselective placement of Au nanoparticles at precise locations on ZnS nanorods through a multi-step reaction sequence that combines partial cation exchange and photodeposition. The placement of the Au nanoparticles on the ZnS nanorods influences their plasmonic properties through controlled average coupling distances. The precision of the cation exchange process is still evolving as we continue to learn more about how these reactions occur and can be controlled. Therefore, while we cannot yet control the precise coupling distance between the photodeposited Au nanoparticles due to limitations in cation exchange capabilities, preliminary results suggest that such control should be possible in the future (Figure S24). Additionally, while this model system was demonstrated using a small palette of materials, a much broader scope of materials is amenable to both cation exchange and photoreduction, making this strategy applicable to other functionally synergistic systems such as photocatalysts, non-linear optical materials, and biosensors.

ASSOCIATED CONTENT

SUPPORTING INFORMATION

Experimental details, additional XRD and UV-Vis data, and individual STEM-EDS elemental maps. This material is available free of charge via the intermet at http://pubs.acs.org.

AUTHOR INFORMATION

Corresponding Author

Raymond E. Schaak – Department of Chemistry, Department of Chemical Engineering, and Materials Research Institute, The Pennsylvania State University, University Park, Pennsylvania 16802, United States; Email: res20@psu.edu

Authors

Joseph M. Veglak – Department of Chemistry, The Pennsylvania State University, University Park, Pennsylvania 16802, United States

Chul-Hyun Jeong – Department of Chemistry, The Pennsylvania State University, University Park, Pennsylvania 16802, United States

Haley L. Young – Department of Chemistry, The Pennsylvania State University, University Park, Pennsylvania 16802, United States

Sarah K. O'Boyle – Department of Chemistry, The Pennsylvania State University, University Park, Pennsylvania 16802, United States

Notes

The authors declare no competing financial interest.

ACKNOWLEDGMENT

This work was supported by the U.S. National Science Foundation under grant CHE-2203353. TEM imaging, X-ray diffraction, and UV-vis-NIR spectroscopy were performed at the Materials Characterization Lab of the Penn State Materials Research Institute. J.M.V. also acknowledges Jennifer Gray and Ke Wang for assistance with electron microscopy and Alex Leffel for assistance with particle counting.

REFERENCES

- (1) Mark, A. G.; Gibbs, J. G.; Lee, T.-C.; Fischer, P. Hybrid Nanocolloids with Programmed Three-Dimensional Shape and Material Composition. *Nature Mater.* **2013**, *12*, 802–807. https://doi.org/10.1038/nmat3685.
- (2) Spear, N. J.; Yan, Y.; Queen, J. M.; Singh, M. R.; Macdonald, J. E.; Haglund, R. F. Surface Plasmon Mediated Harmonically Resonant Effects on Third Harmonic Generation from Au and CuS Nanoparticle Films. *Nanophotonics* **2023**, *12*, 273–284. https://doi.org/10.1515/nanoph-2022-0630.
- (3) Spear, N. J.; Hallman, K. A.; Hernández-Pagán, E. A.; Davidson, R. B.; Arrowood, S. L.; Wistuba, A. L.; Tan, W.; Haglund, R. F.; Macdonald, J. E. Enhanced Broadband and Harmonic Upconversion from Coupled Semiconductor and Metal Nanoparticle Films. *ACS Appl. Nano Mater.* **2020**, *3*, 3144–3150. https://doi.org/10.1021/acsanm.0c00064.
- (4) Metzger, B.; Hentschel, M.; Schumacher, T.; Lippitz, M.; Ye, X.; Murray, C. B.; Knabe, B.; Buse, K.; Giessen, H. Doubling the Efficiency of Third Harmonic Generation by Positioning ITO Nanocrystals into the Hot-Spot of Plasmonic Gap-Antennas. *Nano Lett.* **2014**, *14*, 2867–2872. https://doi.org/10.1021/nl500913t.
- (5) Slablab, A.; Xuan, L. L.; Zielinski, M.; Wilde, Y. de; Jacques, V.; Chauvat, D.; Roch, J.-F. Second-Harmonic Generation from Coupled Plasmon Modes in a Single Dimer of Gold Nanospheres. *Opt. Express, OE* **2012**, *20*, 220–227. https://doi.org/10.1364/OE.20.000220.
- (6) Amirav, L.; Alivisatos, A. P. Photocatalytic Hydrogen Production with Tunable Nanorod Heterostructures. *J. Phys. Chem. Lett.* **2010**, *1*, 1051–1054. https://doi.org/10.1021/jz100075c.
- (7) Di, T.; Xu, Q.; Ho, W.; Tang, H.; Xiang, Q.; Yu, J. Review on Metal Sulphide-Based Z-Scheme Photocatalysts. *ChemCatChem* **2019**, *11*, 1394–1411. https://doi.org/10.1002/cctc.201802024.
- (8) Costi, R.; Saunders, A. E.; Elmalem, E.; Salant, A.; Banin, U. Visible Light-Induced Charge Retention and Photocatalysis with Hybrid CdSe–Au Nanodumbbells. *Nano Lett.* **2008**, *8*, 637–641. https://doi.org/10.1021/nl0730514.
- (9) Levi, A.; Verbitsky, L.; Waiskopf, N.; Banin, U. Sulfide Ligands in Hybrid Semiconductor– Metal Nanocrystal Photocatalysts: Improved Hole Extraction and Altered Catalysis. ACS Appl. Mater. Interfaces 2022, 14, 647–653. https://doi.org/10.1021/acsami.1c17304.
- (10) Storhoff, J. J.; Lazarides, A. A.; Mucic, R. C.; Mirkin, C. A.; Letsinger, R. L.; Schatz, G. C. What Controls the Optical Properties of DNA-Linked Gold Nanoparticle Assemblies? *J. Am. Chem. Soc.* 2000, 122, 4640–4650. https://doi.org/10.1021/ja993825I.
- (11) Elghanian, R.; Storhoff, J. J.; Mucic, R. C.; Letsinger, R. L.; Mirkin, C. A. Selective Colorimetric Detection of Polynucleotides Based on the Distance-Dependent Optical Properties of Gold Nanoparticles. *Science* **1997**, 277, 1078–1081. https://doi.org/10.1126/science.277.5329.1078.
- (12) Storhoff, J. J.; Elghanian, R.; Mucic, R. C.; Mirkin, C. A.; Letsinger, R. L. One-Pot Colorimetric Differentiation of Polynucleotides with Single Base Imperfections Using Gold Nanoparticle Probes. *J. Am. Chem. Soc.* **1998**, *120*, 1959–1964. https://doi.org/10.1021/ja972332i.
- (13) Banin, U.; Ben-Shahar, Y.; Vinokurov, K. Hybrid Semiconductor–Metal Nanoparticles: From Architecture to Function. *Chem. Mater.* **2014**, *26*, 97–110. https://doi.org/10.1021/cm402131n.
- (14) Naskar, S.; Schlosser, A.; Miethe, J. F.; Steinbach, F.; Feldhoff, A.; Bigall, N. C. Site-Selective Noble Metal Growth on CdSe Nanoplatelets. *Chem. Mater.* **2015**, *27*, 3159–3166. https://doi.org/10.1021/acs.chemmater.5b01110.

- (15) Buck, M. R.; Bondi, J. F.; Schaak, R. E. A Total-Synthesis Framework for the Construction of High-Order Colloidal Hybrid Nanoparticles. *Nature Chem.* **2012**, *4*, 37–44. https://doi.org/10.1038/nchem.1195.
- (16) Drake, G. A.; Keating, L. P.; Shim, M. Design Principles of Colloidal Nanorod Heterostructures. *Chem. Rev.* **2023**, *123*, 3761–3789. https://doi.org/10.1021/acs.chemrev.2c00410.
- (17) Hernández-Pagán, E. A.; Lord, R. W.; Veglak, J. M.; Schaak, R. E. Incorporation of Metal Phosphide Domains into Colloidal Hybrid Nanoparticles. *Inorg. Chem.* **2021**, *60*, 4278–4290. https://doi.org/10.1021/acs.inorgchem.0c03826.
- (18) De Trizio, L.; Manna, L. Forging Colloidal Nanostructures via Cation Exchange Reactions. *Chem. Rev.* **2016**. *116*. 10852–10887. https://doi.org/10.1021/acs.chemrev.5b00739.
- (19) Steimle, B. C.; Fagan, A. M.; Butterfield, A. G.; Lord, R. W.; McCormick, C. R.; Di Domizio, G. A.; Schaak, R. E. Experimental Insights into Partial Cation Exchange Reactions for Synthesizing Heterostructured Metal Sulfide Nanocrystals. *Chem. Mater.* **2020**, *32*, 5461–5482. https://doi.org/10.1021/acs.chemmater.0c01388.
- (20) Steimle, B. C.; Fenton, J. L.; Schaak, R. E. Rational Construction of a Scalable Heterostructured Nanorod Megalibrary. *Science* **2020**, *367*, 418–424. https://doi.org/10.1126/science.aaz1172.
- (21) Sadtler, B.; Demchenko, D. O.; Zheng, H.; Hughes, S. M.; Merkle, M. G.; Dahmen, U.; Wang, L.-W.; Alivisatos, A. P. Selective Facet Reactivity during Cation Exchange in Cadmium Sulfide Nanorods. *J. Am. Chem. Soc.* **2009**, *131*, 5285–5293. https://doi.org/10.1021/ja809854q.
- (22) Haynes, C. L.; Van Duyne, R. P. Nanosphere Lithography: A Versatile Nanofabrication Tool for Studies of Size-Dependent Nanoparticle Optics. *J. Phys. Chem. B* **2001**, *105*, 5599–5611. https://doi.org/10.1021/jp010657m.
- (23) Haes, A. J.; Zou, S.; Schatz, G. C.; Van Duyne, R. P. A Nanoscale Optical Biosensor: The Long Range Distance Dependence of the Localized Surface Plasmon Resonance of Noble Metal Nanoparticles. *J. Phys. Chem. B* 2004, 108, 109–116. https://doi.org/10.1021/jp0361327.
- (24) Ringe, E.; McMahon, J. M.; Sohn, K.; Cobley, C.; Xia, Y.; Huang, J.; Schatz, G. C.; Marks, L. D.; Van Duyne, R. P. Unraveling the Effects of Size, Composition, and Substrate on the Localized Surface Plasmon Resonance Frequencies of Gold and Silver Nanocubes: A Systematic Single-Particle Approach. *J. Phys. Chem. C* **2010**, *114*, 12511–12516. https://doi.org/10.1021/jp104366r.
- (25) Chen, A. N.; Scanlan, M. M.; Skrabalak, S. E. Surface Passivation and Supersaturation: Strategies for Regioselective Deposition in Seeded Syntheses. *ACS Nano* **2017**, *11*, 12624–12631. https://doi.org/10.1021/acsnano.7b07041.
- (26) Alemseghed, M. G.; Ruberu, T. P. A.; Vela, J. Controlled Fabrication of Colloidal Semiconductor–Metal Hybrid Heterostructures: Site Selective Metal Photo Deposition. *Chem. Mater.* **2011**, 23, 3571–3579. https://doi.org/10.1021/cm201513a.
- (27) Butterfield, A. G.; Steimle, B. C.; Schaak, R. E. Retrosynthetic Design of Morphologically Complex Metal Sulfide Nanoparticles Using Sequential Partial Cation Exchange and Chemical Etching. *ACS Materials Lett.* **2020**, *2*, 1106–1114. https://doi.org/10.1021/acsmaterialslett.0c00287.
- (28) Zhai, Y.; Flanagan, J. C.; Shim, M. Lattice Strain and Ligand Effects on the Formation of Cu_{2-x}S/I-III-VI₂ Nanorod Heterostructures through Partial Cation Exchange. *Chem. Mater.* **2017**, 29, 6161–6167. https://doi.org/10.1021/acs.chemmater.7b02392.
- (29) Menagen, G.; Macdonald, J. E.; Shemesh, Y.; Popov, I.; Banin, U. Au Growth on Semiconductor Nanorods: Photoinduced versus Thermal Growth Mechanisms. *J. Am. Chem. Soc.* **2009**, *131*, 17406–17411. https://doi.org/10.1021/ja9077733.

- (30) Mokari, T.; Sztrum, C. G.; Salant, A.; Rabani, E.; Banin, U. Formation of Asymmetric One-Sided Metal-Tipped Semiconductor Nanocrystal Dots and Rods. *Nature Mater* **2005**, *4*, 855–863. https://doi.org/10.1038/nmat1505.
- (31) Habas, S. E.; Yang, P.; Mokari, T. Selective Growth of Metal and Binary Metal Tips on CdS Nanorods. *J. Am. Chem. Soc.* **2008**, *130*, 3294–3295. https://doi.org/10.1021/ja800104w.
- (32) Saunders, A. E.; Popov, I.; Banin, U. Synthesis of Hybrid CdS-Au Colloidal Nanostructures. *J. Phys. Chem. B* **2006**, *110*, 25421–25429. https://doi.org/10.1021/jp065594s.
- (33) Hao, J.; Liu, H.; Wang, K.; Sun, X. W.; Delville, J.-P.; Delville, M.-H. Hole Scavenging and Electron–Hole Pair Photoproduction Rate: Two Mandatory Key Factors to Control Single-Tip Au–CdSe/CdS Nanoheterodimers. *ACS Nano* **2021**, *15*, 15328–15341. https://doi.org/10.1021/acsnano.1c06383.
- (34) Suh, I.-K.; Ohta, H.; Waseda, Y. High-Temperature Thermal Expansion of Six Metallic Elements Measured by Dilatation Method and X-Ray Diffraction. *J Mater Sci* **1988**, 23, 757–760. https://doi.org/10.1007/BF01174717.
- (35) Kisi, E. H.; Elcombe, M. M. U Parameters for the Wurtzite Structure of ZnS and ZnO Using Powder Neutron Diffraction. *Acta Cryst C* **1989**, *45*, 1867–1870. https://doi.org/10.1107/S0108270189004269.
- (36) Xu, Y.-N.; Ching, W. Y. Electronic, Optical, and Structural Properties of Some Wurtzite Crystals. *Phys. Rev. B* **1993**, *48*, 4335–4351. https://doi.org/10.1103/PhysRevB.48.4335.
- (37) Fagan, A. M.; Steimle, B. C.; Schaak, R. E. Orthogonal Reactivity and Interface-Driven Selectivity during Cation Exchange of Heterostructured Metal Sulfide Nanorods. *Chem. Commun.* **2022**, *58*, 4328–4331. https://doi.org/10.1039/D1CC07190D.
- (38) Jeffries, W. R.; Fagan, A. M.; Schaak, R. E.; Knappenberger, K. L. Jr. Influence of Band Alignment on Electronic Relaxation in Plasmonic Metal–Semiconductor Hybrid Nanoparticles. *J. Phys. Chem. C* **2022**, *126*, 8384–8392. https://doi.org/10.1021/acs.jpcc.2c01378.